The Journal of Chemical Physics COMMUNICATION scitation.org/journal/jcp

Plasmon-enhanced electrochemical oxidation of 4-(hydroxymethyl)benzoic acid

Cite as: J. Chem. Phys. 157, 081101 (2022); doi: 10.1063/5.0106914
Submitted: 30 June 2022 • Accepted: 27 July 2022 •
Published Online: 22 August 2022

Jingjing Qiu,[a] Daniel Boskin, Dallas Oleson, Weiming Wu, and Marc Anderson

AFFILIATIONS

Department of Chemistry and Biochemistry, San Francisco State University, 1600 Holloway Ave., San Francisco, California 94132, USA

Note: This paper is part of the JCP Special Topic on Plasmon-Driven Energy Conversion.
[a]**Author to whom correspondence should be addressed:** qiu@sfsu.edu

ABSTRACT

Plasmon-mediated electrocatalysis based on plasmonic gold nanoparticles (Au NPs) has emerged as a promising approach to facilitate electrochemical reactions with the introduction of light to excite the plasmonic electrodes. We have investigated the electrochemical oxidation of 4-(hydroxymethyl)benzoic acid (4-HMBA) on gold (Au), nickel (Ni), and platinum (Pt) metal working electrodes in alkaline electrolytes. Au has the lowest onset potential for catalyzing the electrooxidation of 4-HMBA among the three metals in base, whereas Pt does not catalyze the electrooxidation of 4-HMBA under alkaline conditions, although it is conventionally a good electrocatalyst for alcohol oxidation. Both 4-carboxybenzaldehyde and terephthalic acid are detected as the products of electrochemical oxidation of 4-HMBA on the Au working electrode by high-performance liquid chromatography . The electrodeposited Au NPs on indium tin oxide (ITO)-coated glass is further utilized as the working electrode for the 4-HMBA electrooxidation. With its broad absorption in the visible and near-infrared range, we show that the Au NPs on the ITO electrode could enhance the electrochemical oxidation of 4-HMBA under green and red LED light illuminations (505 and 625 nm). A possible reaction mechanism is proposed for the electrochemical oxidation of 4-HMBA on Au working electrodes in an alkaline electrolyte.

INTRODUCTION

The oxidation of alcohols to aldehydes, ketones, and carboxylic acids is a widely used chemical transformation in organic synthesis.[1] The reaction products aldehyde and ketone obtained are broadly used as valued precursors to drugs, fragrances, and aromas. In addition to conventional oxidative routes based on homogeneous reactions with oxidants such as hydrogen peroxide (H_2O_2), a number of new heterogeneously catalyzed processes to selectively oxidize alcohols into carbonyl or carboxyl compounds such as electrochemical oxidation of alcohols have been introduced in the past decade.[2,3] Motivated by electrochemistry's ability to precisely control the flow of electrons in a redox process and its potential to access novel reactions with less expensive and renewable electricity,[4–8] the electrochemical oxidation reactions[3–6] receive increasing attention. It has been shown that the electronic properties of molecules could be modified with the help of an electrode. The chemical properties of the molecule covalently bonded to an electrode were modulated by the applied voltage.[6–8] Recently, the electrochemical oxidation of alcohol molecules has also been applied as an alternative anodic reaction to replace the kinetically sluggish water oxidation reaction/oxygen evolution reaction (OER) in the electrolytic production of hydrogen gas (H_2) or carbon dioxide (CO_2) reduction.[5,9–13] Alcohol electrooxidation driven with lower potential than OER as the anode reaction would, thus, potentially lower the energy requirements for the reduction of water and CO_2 in electrolysis.

In electrochemical oxidation of alcohols, Au metal and Au nanoparticles (NPs) have been proven to be effective electrocatalysts, especially in alkaline electrolytes.[14,15] Au could oxidize a variety of organic alcohols in the absence of harsh chemicals or reaction conditions.[14,16] This electrochemical oxidation involves interfacial proton–electron transfer, and it depends on both pH and the electrode potential.[14,17] In addition to these two factors, it was discovered that Au NPs, which have dual attributes of electrochemical alcohol oxidation activity and visible-light-harvesting ability due

to their localized surface plasmon resonances could further boost the electrochemical reactions.[18–21] The surface plasmon resonance (SPR) of Au NPs was shown to directly enhance the electrooxidation of the hydroxyl groups of the glucose molecules.[18,20] It was proposed that the oxidative hydroxide adsorption on Au NPs and the electrochemical oxidation of glucose were enhanced by the nonthermal charge carriers generated by the plasmon resonance of Au NPs.[20] Similarly, the direct plasmonic charge transfer of a nanoporous Au electrode with broadband absorption was shown spectroscopically to directly facilitate electrochemical water oxidation via the increased adsorbed hydroxide on Au and reactive holes.[21] When coupled with the nickel hydroxide ($Ni(OH)_2$) electrocatalyst, the SPR of Au NPs indirectly enhanced electrochemical water oxidation via charge transfers to the catalyst.[22,23]

Plasmon-mediated electrocatalysis, i.e., the strategic combination of electrocatalysts and plasmonic nanostructures, is emerging as a novel paradigm for improving the overall performance of electrocatalytic processes and has attracted significant interest in the past few years due to its promise for enhancing the efficiency and/or selectivity of electrochemical reactions.[19,24] However, the methodology is still in its infancy and is an underexplored field presenting new opportunities for sustainable production of fuels and value-added chemicals.[18,20,25,26] Despite its great promise, the mechanism of the plasmonic enhancement of electrocatalytic systems, especially the energy transfer across the interface of the plasmonic nanostructures and the reactant molecules, remains poorly understood.[27,28]

Here, we will employ the electrochemical oxidation of 4-(hydroxymethyl)benzoic acid (4-HMBA) as the model reaction on Au and Au NP electrodes. Au NPs electrodeposited on the ITO-coated glass (referred to as Au NP electrode in the paper) will be used as the plasmonic electrode to drive the 4-HMBA electrooxidation. The surfactant-free Au NP electrodes are expected to have dual functions of catalyzing the electrochemical oxidation of the benzyl alcohol derivative 4-HMBA and absorbing visible light due to their surface plasmon resonance. For several Au-catalyzed alcohol oxidation reactions in base, the first deprotonation step was proposed to be catalyzed by hydroxide (OH^-) anions in alkaline solutions, which react with the alcohol to form a reactive alkoxide species ($R\text{-}O^-$) that promotes the overall reaction rate.[14,17] In addition to the hydroxide anions in the basic electrolyte, first-principles calculations predict that the activity and selectivity of alcohol electrooxidation are controlled by the presence of Au surface-adsorbed hydroxyl groups ($Au\text{-}OH_{ads}$) using glycerol as the model system.[29] Both $Au\text{-}OH_{ads}$ and Au can be active sites and are critical in cooperatively facilitating the electrochemical oxidation of alcohols.[29] It was recently demonstrated by *in situ* surface-enhanced Raman scattering (SERS) that the illumination of plasmonic nanoporous Au electrode causes an increased equilibrium coverage of $Au\text{-}OH_{ads}$, which was shown to directly enhance the electrocatalytic water oxidation.[21] We, thus, hypothesize that the Au NP electrodes could catalyze the electrochemical oxidation of the alcohol molecule 4-HMBA in alkaline electrolytes, and its SPR property would further enhance the reaction under resonant light illuminations. We will investigate the electrochemical oxidation of 4-HMBA on a standard Au metal working electrode and then study the SPR effects of an Au NP electrode on this reaction.

RESULTS AND DISCUSSION

The electrochemical oxidation of 4-HMBA can be achieved through conventional electrocatalysis by applying a sufficiently positive bias to the working electrode in an aqueous alkaline electrolyte containing 4-HMBA molecules. The electrochemical oxidation of 4-HMBA was first conducted with standard metal disk working electrodes in a three-electrode cell. The electrolyte was 10 mM 4-HMBA dissolved in 0.1M KOH. A Pt wire was used as the counter electrode and an Hg/HgO electrode as the reference. Cyclic voltammograms (CVs) in the alkaline electrolyte (0.1M KOH and 0.1M KOH +10 mM 4-HMBA) were collected on the Au, Ni, and Pt disk (diameter 1.6 mm) working electrodes, respectively.

As shown in Fig. S1(a), the CV of an Au metal disk working electrode in 0.1M KOH (pH 13) exhibited a broad oxidation peak from 0.4 V vs Hg/HgO [1.3 V vs reversible hydrogen electrode (RHE)] in the anodic scan (i.e., the forward scan). Electrochemical oxidation of the Au metal surface has been well studied, and the broad oxidative peak is attributed to the hydrous oxide formation.[30] The hydroxide anions (OH^-) in the electrolyte could first chemisorb on Au and form $Au\text{-}OH_{ads}$ as shown in Eq. (1). $Au\text{-}OH_{ads}$ will be further oxidized at more positive potentials to produce gold oxide AuO_x [Eq. (2)]. The reduction peak of the oxidized Au was observed at 0.25 V vs Hg/HgO (1.15 V vs RHE) in the cathodic scan (i.e., the reverse scan). When 4-HMBA molecules were added to the alkaline electrolyte [Fig. 1(a) blue curve], two broad oxidation peaks centered at ~0.2 and 0.38 V vs Hg/HgO were observed in the anodic scan. The onset potential of the oxidation peaks was located at −0.2 V vs Hg/HgO (0.7 V vs RHE). In the cathodic scan, an oxidation peak was observed with a peak maximum at 0.18 V vs Hg/HgO (1.1 V vs RHE). The oxidation peak in the cathodic scan is narrower and higher compared with the one in the anodic scan. The CVs of

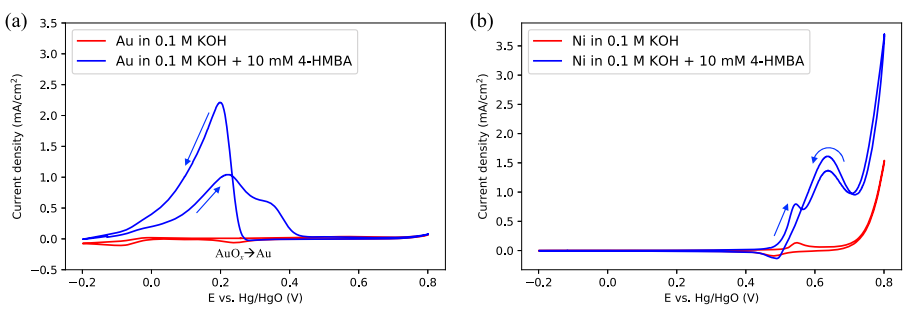

FIG. 1. CVs of Au and Ni working electrodes in alkaline solutions. (a) CVs of an Au disk working electrode in 0.1M KOH (red) and 0.1M KOH with 10 mM 4-HMBA (blue). (b) CVs of a Ni disk working electrode in 0.1M KOH (red) and 0.1M KOH with 10 mM 4-HMBA (blue). The scan rate is 10 mV/s.

alcohol molecules catalyzed by noble metals usually show oxidation peaks in both the anodic scans and the cathodic scans. It was proposed that in the anodic scan the Au-OH_{ads} catalyzes the oxidation of the alcohol molecules but the more oxidized Au surface (AuO_x) could deactivate the alcohol oxidation reaction and, thus, the oxidation current decreases to zero at very high potentials.[31] Fig. 1(a) (blue curve) shows that the oxidation current decreases to virtually zero beyond 0.4 V vs Hg/HgO in the anodic scan, which is attributed to the loss of activity induced by the oxidation of the Au surface. Once AuO_x is reduced according to Eq. (3) in the cathodic scan starting from ~0.28 V vs Hg/HgO, the oxidation peak of 4-HMBA emerges [Fig. 1(a), blue curve]. The onset of the oxidation peak of 4-HMBA in the cathodic scan matches the onset of the Au reduction peak at ~0.28 V vs Hg/HgO [Fig. 1(a), blue curve]. From this observation, we attribute the initiation of the oxidation of 4-HMBA in the cathodic scan to the reactivation of the electrode surface triggered by the reduction of AuO_x to Au. The positive current in the cathodic scan thus has the contributions from both the positive current of the 4-HMBA oxidation and the negative current of the AuO_x reduction. Although there is still debate on the origin of the relative magnitude of the two oxidation peaks of alcohols in the CV, it was proposed that the oxidation peak in the cathodic scan could serve as an indicator of the reactivation of the Au surface via reduction,[31]

$$Au + OH^- \rightarrow Au - OH_{ads} + e^-, \quad (1)$$

$$Au - OH_{ads} + OH^- \rightarrow AuO_x + H_2O + e^-, \quad (2)$$

$$AuO_x + H_2O + 2e^- \rightarrow Au + 2OH^-. \quad (3)$$

Compared with Au, the surface of Ni could be oxidized to $Ni(OH)_2$ and nickel oxyhydroxide (NiOOH) in the alkaline electrolyte under oxidizing potentials.[32] The oxidation peak of Ni into $Ni(OH)_2$ and NiOOH was observed at around 0.58 V vs Hg/HgO and the reduction peak occurred at 0.52 V vs Hg/HgO [Fig. 1(b), red curve]. These redox waves are typical of the electrochemical transformation between $Ni(OH)_2$ and NiOOH on Ni surface.[32,33] $Ni(OH)_2$/NiOOH is known as an active electrocatalyst toward the OER in alkaline electrolytes, and an OER current was indeed observed at potentials higher than 0.7 V vs Hg/HgO in Fig. 1(b) (red curve) with an overpotential of ~340 mV. When 4-HMBA molecules were added to the KOH electrolyte, an additional oxidation peak was observed in the anodic scan at 0.63 V vs Hg/HgO (1.53 V vs RHE) following the oxidation of Ni [Fig. 1(b), blue curve]. This peak is, thus, assigned to the electrooxidation of 4-HMBA, which is similar to the electrochemical oxidation of benzyl alcohol catalyzed by $Ni(OH)_2$/NiOOH.[34] In the cathodic scan, an oxidation peak at the same potential was observed with a higher intensity. It is worth mentioning that the redox waves of Ni grew with scans in the CV, indicative of the electrochemical activation and transformation of more Ni cations into the $Ni(OH)_2$/NiOOH form [Fig. S1(b)]. The current of electrochemical oxidation of 4-HMBA also increased as a result of this electrochemical transformation of Ni [Fig. S1(b)]. When comparing the CVs in Figs. 1(a) and 1(b), the onset potential of the electrooxidation of 4-HMBA is 0.8 V more cathodic on an Au working electrode than on a Ni working electrode. While the oxidation potentials of 4-HMBA are different in the anodic and cathodic scans on Au, they are the same on Ni. In contrast to the results observed with Au and Ni, a Pt disk working electrode showed negligible activity of electrochemical oxidation of 4-HMBA under alkaline conditions (Fig. S2) although Pt is conventionally a good catalyst for alcohol oxidation.[35]

Among all three working electrodes mentioned above, Au shows the lowest onset potential for the electrochemical oxidation of 4-HMBA. This anodic reaction of 4-HMBA electrooxidation was then coupled with a cathodic hydrogen evolution reaction (HER) in an electrolytic cell using an ElectroSyn 2.0 system. The anode was set to be Au and the cathode was Pt. In the non-separated electrolytic cell, the electrolyte was 10 mM 4-HMBA in 0.1M KOH and the potential applied was 2.0 V. The steady-state current for the electrolytic reactions under a fixed potential is summarized in Table S1. After a 3 h reaction in which Au was used as the anode, the solution was analyzed with high-performance liquid chromatography (HPLC). The reactant 4-HMBA and possible oxidized products 4-carboxybenzaldehyde and terephthalic acid were analyzed by HPLC. The retention times of 4-HMBA, 4-carboxybenzaldehyde, and terephthalic acid were determined to be 2.8, 3.7, and 3.1 min, respectively (Fig. S3). Based on these retention times, the molecules in the solution after the 3 h electrolysis with the Au anode were determined to be 52% 4-HMBA, 19% 4-carboxybenzaldehyde and 29% terephthalic acid [Fig. S3(d)]. As a control experiment, the electrolysis was conducted with Ni as the anode and Pt as the cathode with the same electrolyte, the electrolytic current was ~3.5 times lower than that with an Au anode (Table S1).

To further explore the SPR effects of Au NPs on the electrochemical oxidation of 4-HMBA with light, a working electrode was fabricated by electrodepositing Au NPs onto an ITO-coated-glass electrode. Au NPs were cathodically electrodeposited using tetrachloroauric(III) acid ($HAuCl_4$) as the precursor in sulfuric acid (H_2SO_4) following a reported protocol[36] to avoid the presence of surfactant molecules. The surface of the transparent ITO electrode became darker upon the electrodeposition of Au NPs. The surface morphology of the Au NP electrode was characterized by a scanning electron microscope (SEM). As shown in Fig. S4(b), the electrodeposited Au NPs on the ITO surface exhibit long-range uniformity. These electrodeposited nanostructures on the surface of ITO are flower-shaped nanostructures [Figs. 2(a) and S4(c)], and these Au nanoflowers will be referred to as Au NPs in this work regardless of their shapes. The absorbance of the electrode was analyzed by measuring its diffuse reflectance and is shown in Fig. 2(b). It can be seen that the electrode has a broad and continuous absorbance in the visible and NIR range from 500 to 800 nm.

The electrochemical property of the Au NP electrode was then analyzed in the alkaline electrolyte (0.1M KOH). The CV of an Au NP electrode in Fig. 3(a) (blue curve) shows redox waves centered at 0.4 V vs Hg/HgO for the redox events between Au and AuO_x, similar to the ones of an Au disk working electrode [Fig. S1(a)]. With a geometric surface area of the electrode being ~1 cm^2, the electrocatalytic surface area (ECSA) of a typical Au NP electrode was estimated based on a previous report (details shown in the supplementary material) to be about 0.2 cm^2, and the ECSA was used to calculate the current density.[19] Similar to an Au disk working electrode, the Au NP electrode catalyzes the electrochemical oxidation of 4-HMBA but with a higher efficiency reflected by the higher current density, especially in the cathodic scan [Fig. 3(b)]. Since Au

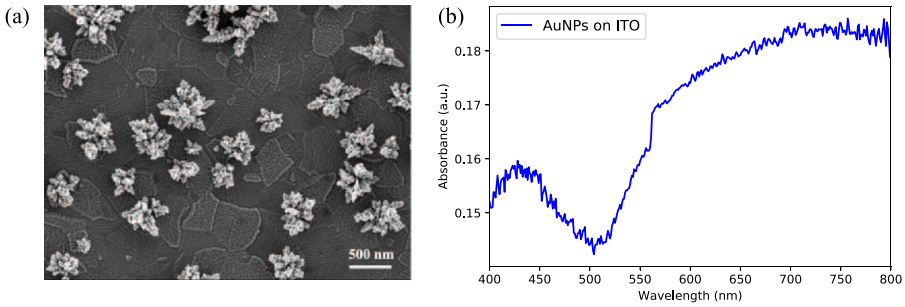

FIG. 2. Surface morphology and optical property of the Au NPs on the ITO electrode. (a) SEM image of the electrodeposited Au nanostructures on the ITO electrode and (b) the diffuse reflectance spectrum of the electrodeposited Au nanostructures on the ITO electrode.

NPs grown on the ITO substrate show a broad absorption in the visible and NIR range, two LED light sources (505 and 625 nm) were chosen for the illuminated electrochemical measurements. The output power of the 505 nm LED was 520 mW but the illumination power on the Au NP electrode surface was attenuated by the electrochemical cell and a layer of 5 mm-thick electrolyte. When the front side of the electrode was illuminated with a 505 nm LED light, the peaks for the Au/AuO_x redox waves did not change [Fig. 3(a)]. The electrocatalytic activity of the Au NP electrode was then tested for the electrochemical oxidation of 10 mM 4-HMBA in 0.1M KOH. When the 505 nm LED light illuminated the front side of the Au NP electrode immersed in the electrolyte containing 4-HMBA, the oxidation peaks in both the anodic and the cathodic scans were higher compared with those under room light [Fig. 3(b)]. The photocurrent, which is defined as the difference between the current density under LED illumination and the current density under room light, depends on the applied potentials (Fig. S5). The highest photocurrent (0.45 mA cm^{-2}) occurred at the potentials of the oxidation of 4-HMBA and no photocurrent was observed above 0.45 V vs Hg/HgO when the alcohol electrooxidation is deactivated due to the oxidation of Au. This enhancement in oxidation current was confirmed in repeated cycles to exclude the potential current change due to electrochemical cycling (Fig. S6). As a control experiment, the Au disk working electrode was also illuminated with the same 505 nm LED light but no enhancement in the currents was observed (Fig. S7).

As shown in Fig. 2(b), the Au NP electrode has a higher absorbance in the NIR range compared with the visible one. A LED with a wavelength of 625 nm was then applied as the illumination source with an output power of 920 mW. Although the illumination power on the Au NP electrode surface was attenuated by the electrochemical cell and a layer of 5 mm-thick electrolyte, positive photocurrents of 4-HMBA electrooxidation on the electrode was observed under this NIR light illumination [Fig. 4(a)]. The increases in currents with a 505 nm LED and a 625 nm LED show a similar potential dependence, and the enhancement is, thus, attributed to the excitation of the SPR effects of the Au NP electrode by the LED lights. It is known that the SPR effects of Au NPs could lead to several outcomes such as enhanced electromagnetic field (i.e., local field enhancement),[37] elevated surface temperature of the nanoparticles (i.e., photothermal effect),[38,39] and generation of energetic charge carriers (i.e., "hot" electrons and holes).[24–27,40] To further determine the possible SPR effects resulting in this enhancement of 4-HMBA electrooxidation observed on Au NP electrodes, the illumination power of the 625 nm LED light source was adjusted. As shown in Fig. 4(b), the current density of electrochemical oxidation of 4-HMBA on the Au NP electrode increases with the increase of the illumination power of the 625 nm LED. It is expected that the strength of SPR effects depends on the illumination power.[27] Figure 4(b) shows the currents of the electrochemical oxidation of 4-HMBA varies with the illumination power and it confirms the impacts of the SPR effects on this reaction. The first possible mechanism of SPR-induced enhancement to consider is the enhanced local electromagnetic field on the surface of the Au NP electrode. Since colorless 4-HMBA electrolyte does not absorb visible or NIR light, the local electromagnetic-field-induced enhancement could be excluded. The possible photothermal effect owing to SPR of the Au NP electrode was then studied by collecting the CVs of a standard Au disk electrode in the electrolyte of 10 mM 4-HMBA in KOH at varying temperatures, even though the temperature of

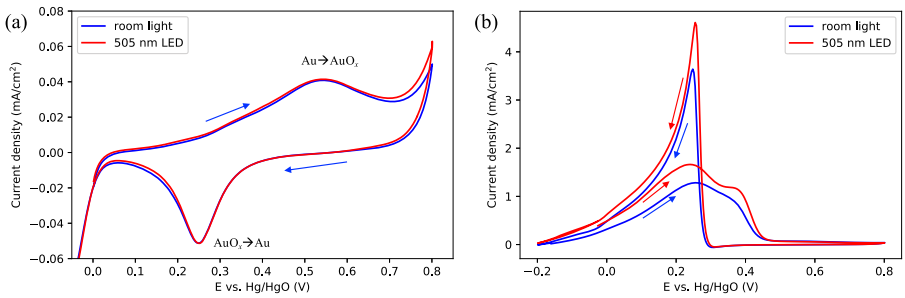

FIG. 3. CVs of an Au NP on ITO working electrode in the different electrolyte. (a) CVs of the Au NP electrode in 0.1M KOH solution. (b) CVs of the Au NP electrode in 10 mM 4-HMBA dissolved in 0.1M KOH. The blue curves are the room light and the red curves are a 505 nm LED illumination (520 mW). The scan rate is 10 mV/s in all scans.

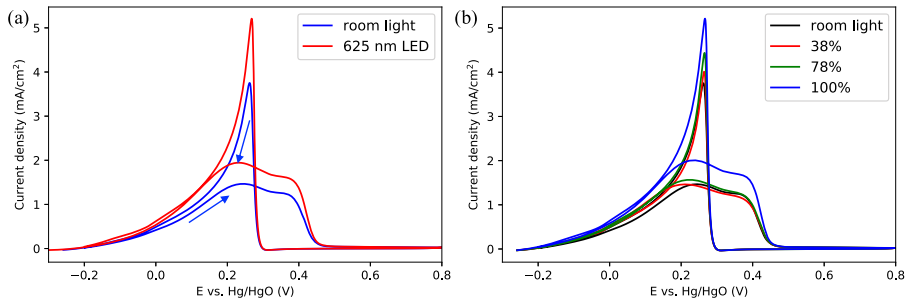

FIG. 4. Electrochemical oxidation of 4-HMBA on an Au NP electrode under the illumination of a 625 nm LED light source. (a) CVs of the electrochemical oxidation of 4-HMBA (10 mM in 0.1M KOH) on an Au NP electrode under room light and a 625 nm-LED light illumination. (b) CVs of the electrochemical oxidation of 4-HMBA (10 mM in 0.1M KOH) on an Au NP electrode under a 625 nm-LED light illumination of different powers. The output power at 100% capacity is 920 mW. The scan rate in all the scans is 10 mV/s.

the bulk electrolyte solution did not change after the LED illuminations. It was shown in Fig. S8(a) that an elevated temperature shifts the reduction peak of AuO_x to less cathodic (more positive) values and the reduction peak size becomes bigger at a higher temperature. For the molecule 4-HMBA [Fig. S8(b)], the onset potential of the oxidation peak on the standard Au disk electrode in the cathodic scan shifts to more cathodic (more positive) values as well and the oxidation peak sizes increase with increasing temperatures. Such peak shifts in CVs caused by pure thermal effects are not observed in the illumination-power-dependent CVs of 4-HMBA, and, thus, the SPR photothermal effect as the sole contributor was excluded for the observed current enhancement in 4-HMBA electrooxidation. Furthermore, the onset potential of 4-HMBA oxidation in the cathodic scan shifts in the same direction with the onset of AuO_x reduction when the solution temperature increases, implying the importance of the role of reactivation of the Au surface in the oxidation of 4-HMBA. Based on the analysis, we tentatively attribute the SPR-enhanced electrochemical oxidation of 4-HMBA on the Au NP electrode to the nonthermal effect, which could be similar to the direct charge transfer observed on the Au nanoporous electrode to water molecules[21] and the electrochemical oxidation of glucose molecules enhanced by the Au NPs.[20]

To further understand the electrochemical oxidation of 4-HMBA catalyzed by Au, the impact of the electrolyte pH was first investigated. Figure S9 shows the CVs of an Au disk electrode and an Au NP electrode in KOH electrolytes of different pH values. The peaks of the redox waves of Au shift to more cathodic values with the increase in the pH of the electrolyte but the peak sizes do not increase dramatically. In addition to the peak shift with pH, the electrochemical oxidation of 4-HMBA is greatly enhanced on an Au electrode in both scans with a more basic electrolyte (Fig. S10), indicating the importance of OH^- in the 4-HMBA electrooxidation. Following the pH-dependent experiments, the scan-rate-dependent experiments were also conducted. Figure S11 shows that the oxidation currents of the 4-HMBA molecules increase with the scan rate and the square root of scan rate in a similar trend for both the Au disk and Au NP electrodes. This shows that the surface morphology (flat film vs NPs) of Au does not affect the reaction mechanism. To study the impact of the –COOH group of the 4-HMBA on the electrochemical oxidation of 4-HMBA, the benzyl alcohol molecules were electrooxidized on a disk Au electrode as a control experiment under the same condition. It was found that the currents of benzyl alcohol electrooxidation are higher in both the anodic and cathodic scans in the CV compared with those of 4-HMBA electrooxidation (Fig. S12). The electrooxidation of benzyl alcohol on Au is not only more efficient than that of 4-HMBA but also could occur within a wider potential window (Fig. S12). To investigate the interactions between the alcohol molecules 4-HMBA and benzyl alcohol with the Au electrode surface, the surface mass change was recorded with electrochemical quartz crystal microbalance (ECQCM) on a Ti/Au crystal. As shown in Fig. S13, the mass changes of 4-HMBA and benzyl alcohol on the Au electrode surface are different and the potentials of the redox activities of the Au electrode interacting with these two molecules are different. These differences imply that 4-HMBA and benzyl alcohol show different adsorption and desorption behaviors on the surface of Au. One possibility of different interactions of the two alcohol molecules with Au could result from the competitive adsorption of the negatively charged carboxylate group on 4-HMBA. The carboxylate groups could be favorably adsorbed onto the Au surface under anodic potentials.[41] It is suggested that some interaction of the alkoxide with the (hydroxylated) Au surface is mandatory[14] and the competitive adsorption of –COOH could hinder the surface interaction of the alcohol group of 4-HMBA with the Au surface, whereas this competition is absent in the case of benzyl alcohol.

We, thus, propose a reaction mechanism of the electrochemical oxidation of the 4-HMBA molecule over the Au catalyst as shown in Fig. 5 based on our results and previous studies.[9,14,29,42] The carboxyl group (–COOH) of the 4-HMBA molecule is expected to be deprotonated at pH 13 under an open circuit condition. The carboxylate anions ($HOCH_2$-Ph-COO^-) then weakly adsorb on the Au surface because Au is a soft Lewis acid, and the carboxylate anion $HOCH_2$-Ph-COO^- is a hard Lewis base (step 1 in Fig. 5). When the applied potential on the Au surface starts to increase, the hydroxide anions (OH^-) will be chemisorbed on the Au and oxidized to form Au-OH_{ads}, which is electrophilic and can catalyze the alcohol oxidation (step 2 in Fig. 5). For 4-HMBA, the proton of the hydroxyl group can be removed at a moderately positive potential in the alkaline electrolyte and form the alkoxide ($^-OCH_2$-Ph-COO^-)

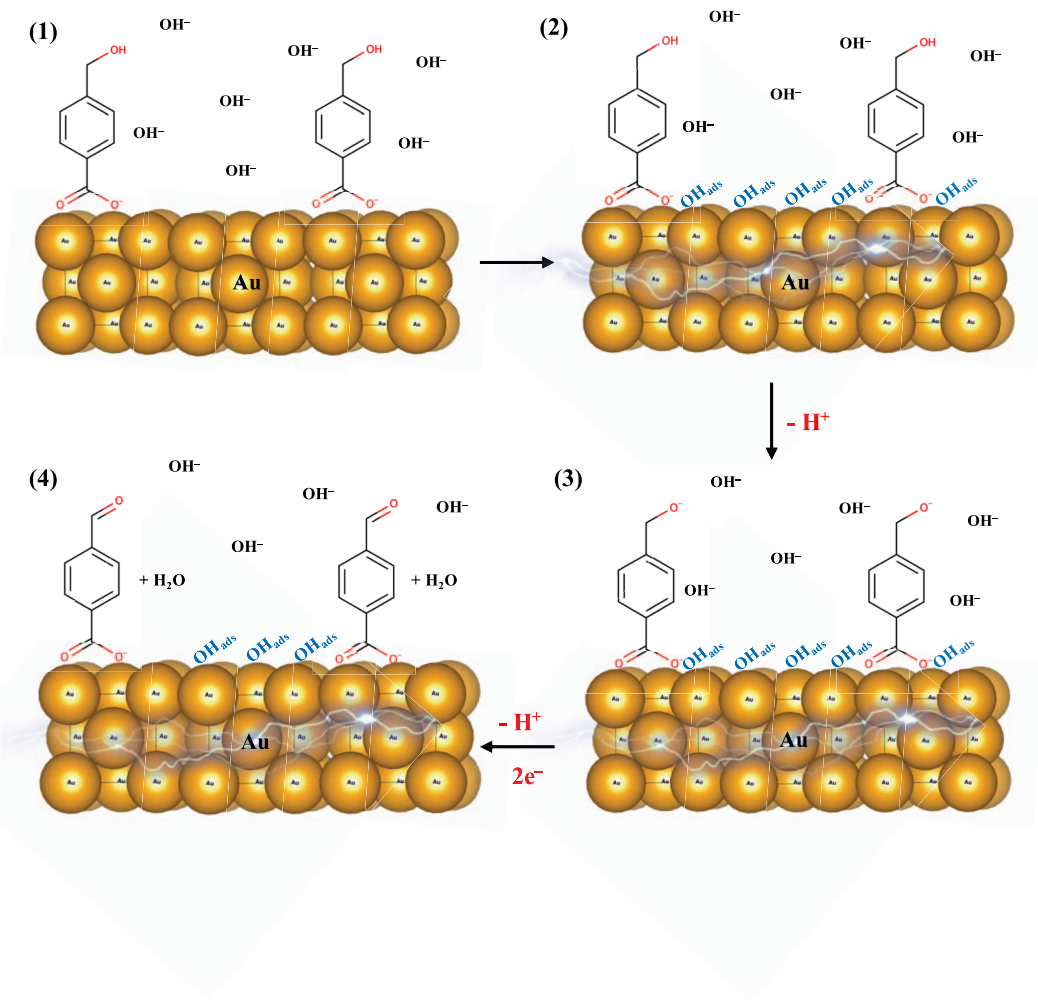

FIG. 5. Schematic illustration of the proposed electrochemical oxidation of 4-HMBA over the Au electrode. (1) adsorption of 4-HMBA molecules on an Au electrode under an open circuit condition; (2) chemisorption of hydroxide anions on an Au electrode at moderately positive potentials; (3) deprotonation of the hydroxyl group of 4-HMBA at positive potentials; and (4) electron-proton transfer of the alkoxide species to form the aldehyde product at positive potentials.

(step 3 in Fig. 5). The alkoxide will then be attacked by the electrophilic Au-OH_{ads} to generate (OHC-Ph-COO^-) and H_2O (step 4 in Fig. 5). The deprotonated 4-carboxybenzaldehyde (OHC-Ph-COO^-) adsorbed on Au surface is not stable in alkaline electrolyte and could be hydrated, which is further oxidized by Au-OH_{ads} to form HOOC-Ph-COO^-. The electrochemical oxidation of 4-carboxybenzaldehyde on an Au electrode is shown in Fig. S14 in which the current in the anodic scan is very low. The HOOC-Ph-COO^- would be further deprotonated in the base to form $^-$OOC-Ph-COO^-. Once Au-OH_{ads} is oxidized to AuO_x, the electrochemical oxidation of 4-HMBA cannot proceed and no current is observed above 0.4 V vs Hg/HgO [Fig. 1(a), blue curve]. The introduction of an Au NP electrode could probably increases the Au-OH_{ads} on the electrode surface by the energetic holes under resonant light illuminations, which enhances the electrochemical oxidation of 4-HMBA.

CONCLUSION

In summary, we have demonstrated the electrochemical oxidation of 4-HMBA molecules on an Au metal electrode and an ITO electrode decorated with electrodeposited Au NPs. The surface redox chemistry of Au plays a critical role in driving the electrochemical oxidation of 4-HMBA. Both Au metal and Au NPs catalyze the electrooxidation of 4-HMBA molecules effectively in alkaline electrolytes, and a higher pH is beneficial for this electrooxidation reaction. Both 4-carboxybenzaldehyde and terephthalic acid were detected in the reaction products of 4-HMBA electrooxidation by HPLC. It is further shown that the broad absorption of the Au NP electrode due to its SPR could enhance the electrochemical oxidation of 4-HMBA molecules under visible and NIR light illuminations. It is proposed that the nonthermal charge carriers of the SPR lead to the enhanced electrochemical oxidation of 4-HMBA

on the Au NP electrode by excluding the photothermal and enhanced electromagnetic field effects. The present work endeavors to shed light on the electrochemical oxidation of benzyl alcohol derivatives using 4-HMBA as a model system with Au NP electrodes and the possible reaction enhancement powered by visible and NIR lights. The results are expected to provide insights into designing electrochemical devices using plasmonic metal nanostructures. Future work will focus on investigating the reaction mechanism of the electrochemical oxidation of electronically unique aromatic substituents and the charge transfer mechanisms of the SPR from plasmonic Au nanostructure electrodes in assisting electrochemical reactions.

SUPPLEMENTARY MATERIAL

See the supplementary material for experimental methods and additional table and figures as noted in the main text, including CVs, HPLC data, SEM images, and ECQCM data.

ACKNOWLEDGMENTS

We acknowledge the National Science Foundation (NSF) for the support of the work under Grant No. 2102196. We also acknowledge the NSF for Award No. CHE 0821619, which funded the SEM instrument at San Francisco State University. We also acknowledge the startup fund and the small grant from San Francisco State University in support of this work. We appreciate the assistance from Clive Hayzelden with the SEM characterization and the help from Dr. Andrew Ichimura at San Francisco State University with the diffuse reflectance spectra of the Au NP electrodes.

AUTHOR DECLARATIONS

Conflict of Interest

The authors have no conflicts to disclose.

Author Contributions

Jingjing Qiu: Conceptualization (lead); Data curation (equal); Formal analysis (lead); Funding acquisition (lead); Investigation (lead); Methodology (lead); Project administration (lead); Supervision (lead); Visualization (lead); Writing – original draft (lead); Writing – review & editing (lead). **Daniel Boskin**: Data curation (equal); Formal analysis (supporting); Writing – review & editing (supporting). **Dallas Oleson**: Data curation (supporting); Formal analysis (supporting). **Weiming Wu**: Formal analysis supporting; Investigation (supporting); Writing – review & editing (supporting). **Marc Anderson**: Data curation (supporting); Writing – review & editing (supporting).

DATA AVAILABILITY

The data that support the findings of this study are available within the article and its supplementary material.

REFERENCES

[1]W.-Y. Tan, Y. Lu, J.-F. Zhao, W. Chen, and H. Zhang, Org. Lett. **23**, 6648 (2021).
[2]R. Ciriminna, V. Pandarus, F. Béland, Y.-J. Xu, and M. Pagliaro, Org. Process Res. Dev. **19**, 1554 (2015).
[3]W.-J. Liu, L. Dang, Z. Xu, H.-Q. Yu, S. Jin, and G. W. Huber, ACS Catal. **8**, 5533 (2018).
[4]J. Wang, A. Khaniya, L. Hu, M. J. Beazley, W. E. Kaden, and X. Feng, J. Mater. Chem. A **6**, 18050 (2018).
[5]Z. G. Schichtl, S. K. Conlin, H. Mehrabi, A. C. Nielander, and R. H. Coridan, ACS Appl. Energy Mater. **5**, 3863 (2022).
[6]A. Wiebe, T. Gieshoff, S. Möhle, E. Rodrigo, M. Zirbes, and S. R. Waldvogel, Angew. Chem., Int. Ed. **57**, 5594 (2018).
[7]J. Heo, H. Ahn, J. Won, J. G. Son, H. K. Shon, T. G. Lee, S. W. Han, and M.-H. Baik, Science **370**, 214 (2020).
[8]K. M. Van Geem, V. V. Galvita, and G. B. Marin, Science **364**, 734 (2019).
[9]M. T. Bender, X. Yuan, and K.-S. Choi, Nat. Commun. **11**, 4594 (2020).
[10]D. Wang, P. Wang, S. Wang, Y.-H. Chen, H. Zhang, and A. Lei, Nat. Commun. **10**, 2796 (2019).
[11]B. You and Y. Sun, Acc. Chem. Res. **51**, 1571 (2018).
[12]F. Arshad, T. u. Haq, I. Hussain, and F. Sher, ACS Appl. Energy Mater. **4**, 8685 (2021).
[13]Y. Xu and B. Zhang, ChemElectroChem **6**, 3214 (2019).
[14]Y. Kwon, S. C. S. Lai, P. Rodriguez, and M. T. M. Koper, J. Am. Chem. Soc. **133**, 6914 (2011).
[15]T. Suga, N. Shida, and M. Atobe, Electrochem. Commun. **124**, 106944 (2021).
[16]X. Huang, O. Akdim, M. Douthwaite, K. Wang, L. Zhao, R. J. Lewis, S. Pattisson, I. T. Daniel, P. J. Miedziak, G. Shaw, D. J. Morgan, S. M. Althahban, T. E. Davies, Q. He, F. Wang, J. Fu, D. Bethell, S. McIntosh, C. J. Kiely, and G. J. Hutchings, Nature **603**, 271 (2022).
[17]N. Govindarajan, A. Xu, and K. Chan, Science **375**, 379 (2022).
[18]C. Wang, X.-G. Nie, Y. Shi, Y. Zhou, J.-J. Xu, X.-H. Xia, and H.-Y. Chen, ACS Nano **11**, 5897 (2017).
[19]E. Contreras, R. Nixon, C. Litts, W. Zhang, F. M. Alcorn, and P. K. Jain, J. Am. Chem. Soc. **144**, 10743 (2022).
[20]M. Rodio, M. Graf, F. Schulz, N. S. Mueller, M. Eich, and H. Lange, ACS Catal. **10**, 2345 (2020).
[21]M. Graf, G. B. Vonbun-Feldbauer, and M. T. M. Koper, ACS Nano **15**, 3188 (2021).
[22]S. Wang, Y. Gao, S. Miao, T. Liu, L. Mu, R. Li, F. Fan, and C. Li, J. Am. Chem. Soc. **139**, 11771 (2017).
[23]K. Suzuki, X. Li, T. Toda, F. Nagasawa, and K. Murakoshi, ACS Energy Lett. **6**, 4374 (2021).
[24]J. Zhao, S. Xue, R. Ji, B. Li, and J. Li, Chem. Soc. Rev. **50**, 12070 (2021).
[25]C. H. Choi, K. Chung, T.-T. H. Nguyen, and D. H. Kim, ACS Energy Lett. **3**, 1415 (2018).
[26]H. Robatjazi, S. M. Bahauddin, C. Doiron, and I. Thomann, Nano Lett. **15**, 6155 (2015).
[27]C. Zhan, B.-W. Liu, Y.-F. Huang, S. Hu, B. Ren, M. Moskovits, and Z.-Q. Tian, Nat. Commun. **10**, 2671 (2019).
[28]Y. Yu, V. Sundaresan, and K. A. Willets, J. Phys. Chem. C **122**, 5040 (2018).
[29]A. M. Verma, L. Laverdure, M. M. Melander, and K. Honkala, ACS Catal. **12**, 662 (2022).
[30]S. Yang and D. G. H. Hetterscheid, ACS Catal. **10**, 12582 (2020).
[31]Y. Zhao, X. Li, J. M. Schechter, and Y. Yang, RSC Adv. **6**, 5384 (2016).
[32]L. Trotochaud, S. L. Young, J. K. Ranney, and S. W. Boettcher, J. Am. Chem. Soc. **136**, 6744 (2014).
[33]F. A. L. Laskowski, M. R. Nellist, R. Venkatkarthick, and S. W. Boettcher, Energy Environ. Sci. **10**, 570 (2017).
[34]M. T. Bender, Y. C. Lam, S. Hammes-Schiffer, and K.-S. Choi, J. Am. Chem. Soc. **142**, 21538 (2020).
[35]S. C. S. Lai and M. T. M. Koper, Phys. Chem. Chem. Phys. **11**, 10446 (2009).

[36]K. J. Stine, Appl. Sci. **9**, 797 (2019).
[37]K. A. Willets and R. P. Van Duyne, Annu. Rev. Phys. Chem. **58**, 267 (2007).
[38]Y. Dubi, I. W. Un, and Y. Sivan, Chem. Sci. **11**, 5017 (2020).
[39]Y. Yu, J. D. Williams, and K. A. Willets, Faraday Discuss. **210**, 29 (2018).
[40]J. Song, J. Long, Y. Liu, Z. Xu, A. Ge, B. D. Piercy, D. A. Cullen, I. N. Ivanov, J. R. McBride, M. D. Losego, and T. Lian, ACS Photonics **8**, 1497 (2021).
[41]W.-k. Paik, S. Han, W. Shin, and Y. Kim, Langmuir **19**, 4211 (2003).
[42]Z. Li, Y. Yan, S.-M. Xu, H. Zhou, M. Xu, L. Ma, M. Shao, X. Kong, B. Wang, L. Zheng, and H. Duan, Nat. Commun. **13**, 147 (2022).